Initial Surface Reactions of TiO_2 Atomic Layer Deposition onto SiO_2 Surfaces: Density Functional Theory Calculations

Zheng Hu and C. Heath Turner*

Department of Chemical and Biological Engineering, University of Alabama, Tuscaloosa, Alabama 35487

Received: January 18, 2006; In Final Form: March 2, 2006

We present a density functional theory (DFT) study of the initial surface reactions of TiO_2 deposition onto a SiO_2 substrate using atomic layer deposition (ALD). The precursors for the deposition process were chosen to be $TiCl_4$ and H_2O, and several cluster models were used for the SiO_2 substrate. We predict the activation barriers, transition states, and reaction pathways of the surface reactions, and we investigate the effect of surface heterogeneity (such as the presence of siloxane bridges) on the reactivity of the SiO_2 surface. Our study suggests that the concentration and arrangement of different reactive groups on the substrate will strongly dictate the process of film growth during ALD, including the film morphology and the growth rate.

1. Introduction

Two of the most critical issues currently facing the semiconductor industry are the discovery of high-κ gate dielectric replacement materials for SiO_2 and the development of deposition processes that achieve high surface uniformity and controlled growth at the atomic scale.[1] Atomic layer deposition (ALD) is an ideal candidate for meeting these challenges, enabling thin film growth on various surfaces, ranging from planar substrates to nanoporous materials. The deposition can occur uniformly or may also be patterned on surfaces to create quantum dots (with potential applications as memory devices) or to facilitate the patterning of subsequent layers, such as Cu on a glass substrate.[2] Although ALD was introduced nearly 30 years ago, its utility is growing significantly as desired film thicknesses are shrinking in the electronic materials industry. Valuable film properties, such as excellent conformality, uniformity, and controllability obtained with this technique are now beginning to outweigh the inherent drawback of low deposition rates.

Research groups around the world have just recently begun exploring the properties and potential applications of ALD processing. For instance, within the last year, King and co-workers[3,4] have found that ALD films have enormous potential for attaining high performance photonic crystal structures and optical microcavities. The performance benefits are credited to the highly conformal and uniform coatings achieved during the deposition process. Others have begun experimenting with nanolaminated thin films, synthesized by using alternating precursors during the ALD process.[5] These atomically detailed films have been shown to possess superior characteristics for high-κ gate-oxide materials, which are commonly used in metal-oxide-semiconductor field effect transistors (MOSFETs). There is a huge market potential for the application of ALD processing to microelectromechanical systems (MEMS), due to the precision attainable with this technique. In contrast to the other techniques tested, ALD allows highly conformal coatings to be deposited on high aspect ratio structures, which are typical of MEMS devices.[6] In fact, a recent report[7] has shown that the tribological characteristics of surfaces can be significantly improved through the use of ALD coatings, due to the highly uniform nature of the deposition. This is quantified with respect to the debris creation and the stability of the friction coefficient. In other areas, TiO_2 and other metal oxides have been deposited on the surfaces of anodic aluminum oxide membranes by using ALD, to modify the surface uniformity, surface chemistry, and selectivity of the pores, and the surface coatings have been shown to be stable up to as much as 500 °C in some cases.[8−10] Related to this work, others have found that porous TiO_2 materials can be optimal substrates for biosensing applications.[11] While many other applications of ALD exist, these initial discoveries clearly motivate the need to develop fundamental models and simulation tools to help guide this technique.

Although ALD is now gaining significant interest among a broad research base, a fundamental understanding of this technique at the atomic scale is relatively nonexistent, which severely hampers its future development. We focus on the initial surface reactions of TiO_2 deposition onto a SiO_2 substrate using $TiCl_4$ and H_2O as precursors. While the growth characteristics of these films are pertinent to a wide range of future applications (such as high-κ gate dielectric replacement materials, thin film photocatalysts, dielectric optical filters and waveguides, etc.), a detailed mechanistic study of the surface processes is lacking.

In this work, we present DFT calculations of the initial reaction mechanisms of ALD of TiO_2 onto SiO_2 surfaces using hybrid density functional theory. At the onset, it is important to recognize that we restrict our investigation to modeling only the initial reaction mechanisms. The actual ALD growth mechanism is complicated by competing reactions and significant structural relaxation, as surface coverage increases and subsequent layers are deposited.[12] In fact, the densification processes occurring during ALD thin film growth have been studied by others with Kinetic Monte Carlo (KMC) simulations.[13] The KMC approach is able to capture this behavior, which is accompanied by increasing coordination number of the metal atoms within the deposited film. In addition, the actual growth process depends on the operating conditions and the configurations and densities of surface reactive sites, often leading to amorphous structures and point defects in the deposited film. Due to the high computational cost of first-principle calculations, it is not practical to model all of the features of the ALD growth cycle. Therefore, we focus only on

10.1021/jp060367b CCC: $33.50
Published on Web 04/04/2006

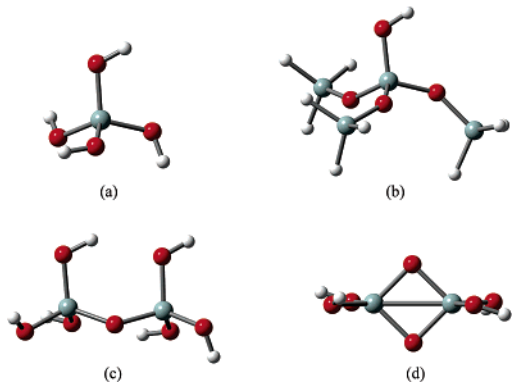

Figure 1. Cluster models used to represent reactive sites on the SiO_2 surface: (a) $Si(OH)_3-OH$ cluster used to represent isolated surface −OH groups, (b) $(SiH_3O)_3Si-OH$ cluster used to represent isolated surface −OH groups, (c) $Si(OH)_3-O-Si(OH)_3$ cluster used to represent adjacent hydrogen-bonded −OH groups, and (d) cluster used to represent siloxane bridge sites on the SiO_2 surface.

the initial surface reaction mechanisms that initialize the ALD growth of TiO_2 on different reactive sites of SiO_2 surfaces in the zero coverage limit. Our DFT calculations suggest that the presence of various surface functionalities will have a significant impact on the film deposition process, and this information should be used to identify suitable experimental operating conditions for achieving a desired film quality. The details of our calculations are presented in the following section.

2. Computational Details

There are two types of reactive sites on the hydroxylated SiO_2 surface: surface −OH groups (Figure 1a−c) and siloxane bridges (Figure 1d). To represent these reaction sites on the surface, several cluster models are used in this work. First, we used a small $Si(OH)_3-OH^*$ cluster (Figure 1a) to represent isolated −OH groups on the surface, where surface species are denoted by asterisks. Next, a larger cluster, $(SiH_3O)_3Si-OH^*$, shown in Figure 1b, is used to investigate cluster size effects. Besides isolated −OH groups, the hydroxylated SiO_2 surface also has adjacent −OH groups normally linked by a hydrogen bond. To investigate surface reactions on the hydrogen-bonded hydroxyl groups, we used the $Si(OH)_3-O-Si(OH)_3$ cluster model shown in Figure 1c.

These models above have also been previously used by Han and co-workers to investigate ZrO_2 ALD growth on a SiO_2 surface.[14] At high temperature, the neighboring −OH groups can also react to give up free water molecules, leaving reactive siloxane bridges, as shown in Figure 1d. The geometry of all four cluster models is optimized without applying boundary constraints. This may underestimate the actual mechanical constraints imposed on the atoms of the cluster, due to binding with the rest of the surface. However, we found that the bonding interactions involved in the surface reactions are sufficiently local and delocalization effects are not significant. As a result, the fully relaxed clusters are sufficient to obtain the relative energies of critical structures for the surface reactions. In addition, we did not observe unrealistic structural reorganization of the cluster models, when compared to their experimental analogues.

Our predicted reaction mechanisms of TiO_2 ALD on the hydroxylated SiO_2 surface are based on accurate first-principles studies of reaction pathways of gaseous precursors interacting with the SiO_2 cluster models. All calculations were performed with Gaussian03.[15] The minimum energy structures and transition structures along surface reaction pathways were computed

TABLE 1: Predicted Relative Energies of the Critical Structures for the $Si(OH)_3-OH^* + TiCl_4 \rightarrow Si(OH)_3-O-TiCl_3^* + HCl$ Half-Reaction Calculated at Three Different Model Chemistries

	relative energy (kcal/mol)		
	MC1	MC2	MC3
$Si(OH)_3-OH^* + TiCl_4$	0	0	0
reactant complex	−8.9	−3.8	−3.2
TS	5.9	10.9	11.2
$Si(OH)_3-O-TiCl_4^* + HCl$	−7.9	−4.6	−4.0

TABLE 2: Predicted Relative Energies of the Critical Structures for the $Si(OH)_3-O-TiCl_3^* + H_2O \rightarrow Si(OH)_3-O-Ti(OH)Cl_2^* + HCl$ Half-Reaction Calculated at Three Different Model Chemistries

	relative energy (kcal/mol)		
	MC1	MC2	MC3
$Si(OH)_3-O-TiCl_3^* + H_2O$	0	0	0
reactant complex	−11.0	−3.4	−3.8
TS	2.1	13.8	12.7
product complex	7.8	−0.3	−0.5
$Si(OH)_3-O-Ti(OH)Cl_2^* + HCl$	−5.3	3.2	2.6

by using gradient-corrected density functional theory with the Becke three-parameter exchange functional[16] and the Lee−Yang−Parr correlation functional[17] (B3LYP). This method has been successfully used to predict reaction mechanisms and associated energetics for a number of reactions in ALD thin film growth.[1,14,18−23] B3LYP has also been shown to be accurate for studying transition metals.[24] To determine the effect of basis set on energy prediction, we performed preliminary calculations of the initial surface reactions between the SiO_2 surface and the precursors $TiCl_4$ and H_2O using the small $Si(OH)_3-OH^*$ cluster. The reaction barriers were predicted by using three model chemistries:

MC1: B3LYP/6-31G(d,p)//B3LYP/6-31G(d,p)

MC2: B3LYP/6-311++G(2df,2p)//B3LYP/6-31G(d,p)

MC3: B3LYP/6-311++G(2df,2p)//B3LYP/6-311++G(2df,2p)

The model to the left of the double slash is the one at which the energy was computed, and the model to the right of the double slash is the one at which the molecular geometry was optimized. While the details of these basis sets and nomenclature can be found elsewhere,[25] the progression from MC1 to MC3 represents a simultaneous increase in model accuracy and computational demand. Our calculations indicated that, although the reaction mechanisms for the two half-reactions do not change with different model chemistries, the reaction energetics are certainly affected. The predicted relative energies of the critical structures along the reaction pathways for the two half-reactions with the three model chemistries are given in Tables 1 and 2.

The predictions from the lowest cost MC1 model chemistry differ significantly from the results from the highest level MC3 model chemistry. The small 6-31G(d,p) basis set[26] for both geometry optimization and energy calculation does not give an accurate energy prediction for the adsorbed complex or the transition state structures. The triple-ζ basis sets, multiple polarization functions, and diffuse functions can significantly improve the description of bond energies, especially for the adsorbed complex and the transition state structures. The MC2 and MC3 model chemistries give very similar results. The $TiCl_4$ adsorption energy on the SiO_2 surface is calculated to be 3.8

and 3.2 kcal/mol, using the MC2 and MC3 model chemistries, respectively. The calculated reaction barrier between $TiCl_4$ and the SiO_2 surface with these two model chemistries is also very similar, with a difference of 0.3 kcal/mol. The largest difference between the results obtained from the two model chemistries is observed in the reaction barrier of the second half-reaction between H_2O and $Si(OH)_3-O-TiCl_3$*, which is only 0.7 kcal/mol. The MC2 model chemistry, which performs the energy calculation with the large 6-311++G(2df,2p) basis set[27,28] at the geometry optimized with the small 6-31G(d,p) basis set, yields very similar results to those with the higher cost MC3 model chemistry. Therefore, the B3LYP/6-311++G(2df,2p)//B3LYP/6-31G(d,p) model chemistry was used in all of our subsequent calculations due to an optimal tradeoff between computational accuracy and resource cost.

Corrections for basis set superposition error (BSSE) were estimated by the counterpoise method[29] in preliminary tests. Our calculations on the small model (Figure 1a) suggest that in computing the binding energy of the reactant and product complexes, the use of MC1 model chemistry leads to a large BSSE. This is primarily due to the negatively charged O atoms, which borrow the basis functions available on the Ti atom. This leads to a more flexible description of the wave function and ultimately a lower energy of the adsorbed complexes, which can be incorrectly ascribed to an increase in the binding energy. Although the difference between the uncorrected and the BSSE corrected binding energies is rather large in the case of small basis sets, it becomes much smaller by using larger basis sets: 0.8−1.3 and 1.2−1.5 kcal/mol at MC2 and MC3 model chemistries, respectively. At the B3LYP level, the triple-ζ basis sets, multiple polarization functions, and diffuse functions reduce the BSSE to a negligible level. Therefore, in the following consideration, we use the MC2 model chemistry without BSSE corrections.

Gaussian03's reaction path following facility was used to explore the reaction potential energy surfaces (PES). Geometries were optimized by minimizing the energy to stationary points on the PES. The nature of the calculated structures was verified by subsequent frequency calculations, which also yielded zero-point energy (ZPE) corrections. Intrinsic reaction coordinate (IRC) calculations were performed to examine the reaction path leading down from a transition structure in both directions on the PES to ensure that the transition states connect reactants to products. The normal modes corresponding to the imaginary frequencies of the transition state structures were examined with molecular visualization to verify that the nuclear motion tends to deform the transition state structure along the pertinent reaction coordinate.

3. Results and Discussion

ALD growth of TiO_2 from $TiCl_4$ and H_2O involves alternating exposure of the two precursors. Thus, the growth of TiO_2 involves two half-reactions:

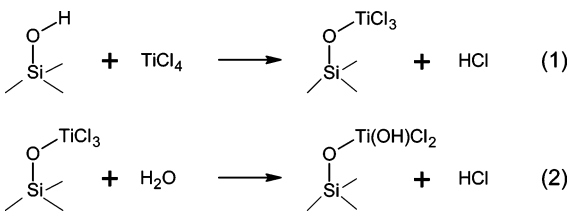

The actual reactions taking place during each exposure depend on a number of factors, such as temperature, surface coverage, and the presence of reactive sites on the surface, which we examine in some detail here. Different types of reactive functional groups exist on the SiO_2 surface and they may have different reaction mechanisms with the gaseous precursors. In the following sections, we present DFT calculations of the initial reaction mechanisms between different surface active groups and the precursors, $TiCl_4$ and H_2O.

3.1. Isolated Hydroxyl Groups. *3.1.1. First Half-Reaction.* The reaction of $TiCl_4$ with surface −OH groups is initiated by the adsorption of $TiCl_4$ onto the surface. A relaxed PES scan (which samples points on the potential surface and performs a geometry optimization of the remaining nonscanned coordinates) indicates that there is not a barrier for the adsorption of $TiCl_4$ onto the surface −OH groups. $TiCl_4$ spontaneously adsorbs onto the isolated −OH surface sites through Lewis acid/base interactions between Ti and O to form a reactant complex with a Ti−O bond distance of 2.28 Å. A natural bond orbital (NBO) calculation was carried out to examine the interaction between $TiCl_4$ and the surface −OH groups. The second-order perturbation theory analysis shows that the interactions between the oxygen lone pair NBO and the Ti−Cl antibond NBOs give strong stabilization. These interactions lead to donation of occupancy from the oxygen lone pair NBO into the empty Ti−Cl antibond hybrid orbitals.

A natural population analysis yields consistent results. The total population on all of the natural atomic orbitals (NAO) of $TiCl_4$ increased by 0.11 in the adsorbed state compared to that in the gas phase. The occupancy donated by the oxygen of the surface hydroxyl group is delocalized in the NAOs of $TiCl_4$. This interaction leads to an approximate 5-coordination Ti and changes the coordination geometry from tetrahedron close to trigonal bipyramid. The adsorption step is weakly exothermic with an adsorption energy of −3.2 kcal/mol.

Following the formation of the adsorbed complex, Ti in the $TiCl_4$ can attack the O in the surface −OH to release HCl through a transition state, as shown in Figure 2c. As Ti approaches O, electronic charge is transferred from O (donor) to Ti (acceptor) with the formation of a Ti−O bond. The accumulation of negative charge on Ti can induce the rehybridization of the Ti group from 5-coordination to 4-coordination, which leads to the breakage of one Ti−Cl bond, releasing a negatively charged Cl. Meanwhile, the rehybridization of the Ti group stabilizes a buildup of negative charge on the O and weakens the O−H bond. When the negatively charged Cl that is released "sees" the positively charged H in the transition state structure, it promptly attacks the weakened O−H bond, leading to the breakage of the O−H bond and the formation of the H−Cl bond. The reaction mechanism above is illustrated in Figure 2. The energy profile for this first half-reaction on the isolated hydroxyl group is shown in Figure 3. As indicated in the figure, this reaction is exothermic by 6.5 kcal/mol, with an activation barrier of 11.9 kcal/mol. The HCl product molecules that are formed may adsorb on the surface, but they can be easily desorbed due to their weak binding energy (0.4 kcal/mol).

3.1.2. Second Half-Reaction. During the exposure of water, water molecules react with the surface intermediates deposited during the first half-cycle to release additional HCl species. The water molecules first approach the surface to form weakly adsorbed complexes through a Lewis acid/base interaction between Ti and O. The adsorption of water can occur in different modes, such as attached to the top or side sites of Ti intermediates. The three water adsorption states (RC1, RC2, and RC3) that have been identified are shown in Figure 4, and these correspond to local minima on the potential energy surface.

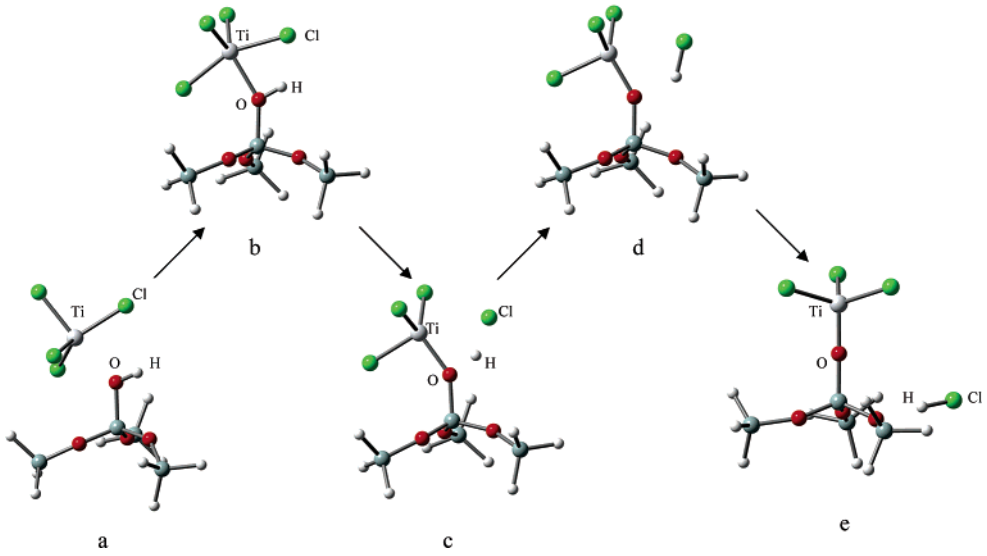

Figure 2. Atomic mechanism of the reaction between $TiCl_4$ and the isolated surface −OH group: (a) reactant complex, (b) formation of the Ti−O bond and the 5-coordinated Ti, (c) transition state structure, (d) formation of the H−Cl bond, and (e) product complex.

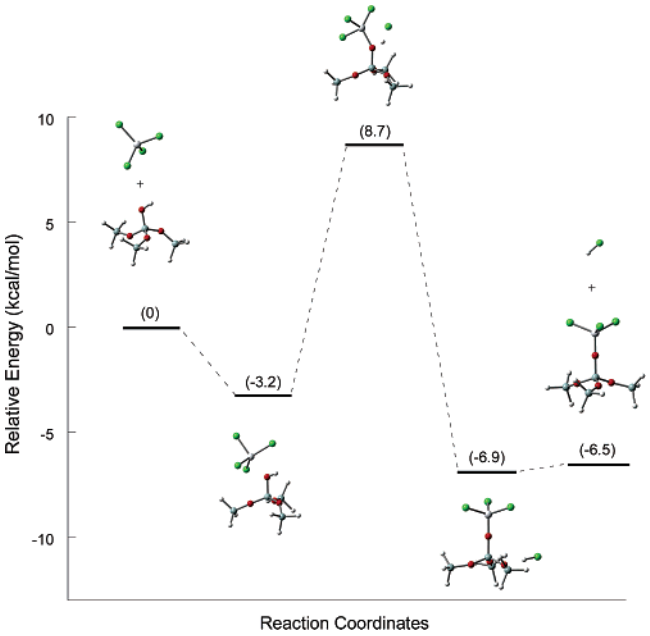

Figure 3. ZPE-corrected potential energy surface for the $(SiH_3O)_3$-Si−OH* + H_2O reaction, calculated by using the MC2 model chemistry.

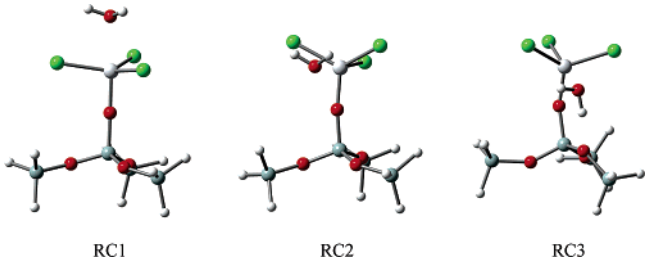

Figure 4. Adsorbed complex structures optimized at the B3LYP/6-31G(d,p) level of theory. RC1, RC2, and RC3 are the three different adsorption modes of H_2O on the SiO_2−O−$Ti(OH)_3$* surface site.

The binding energies for adsorption are predicted to be −3.7 (RC1), −2.8 (RC2), and −2.0 (RC3) kcal/mol. The weakly adsorbed water molecules can diffuse on the surface and change from one adsorption state to another. The activation energy of the diffusion is 0.6 kcal/mol from RC3 to RC2 and 2.7 kcal/mol from RC2 to RC1. These two steps are exothermic by 0.8 and 0.9 kcal/mol, respectively. The energy barrier of the reverse diffusion is not much higher, 1.4 kcal/mol from RC2 to RC3 and 3.6 kcal/mol from RC1 to RC2. The small "hop" barriers and the nearly equivalent potential energies of the three adsorbed states make the diffusion among all of the different adsorption states possible. Thus, there is not a significant preference among the different adsorption modes, suggesting an equilibrium distribution of adsorbed states.

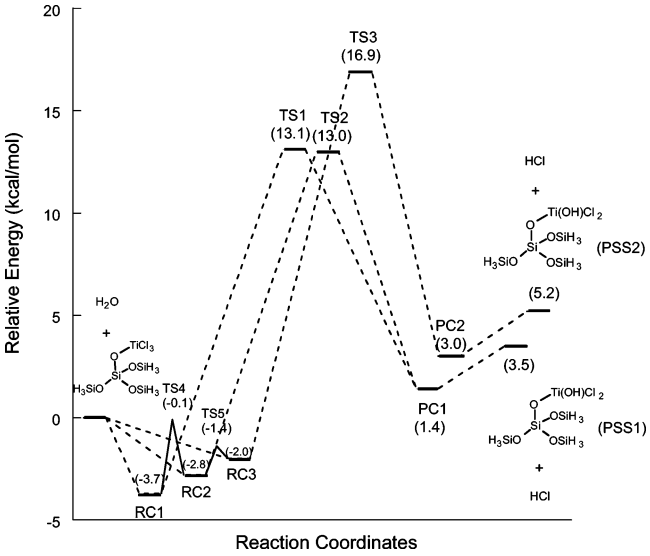

Figure 5. ZPE-corrected PES for the surface diffusion of H_2O and the $(SiH_3O)_3Si$−O−$TiCl_3$* + H_2O reaction. RC1, RC2, and RC3 are the three different reactant complexes formed by the different adsorption modes of H_2O. TS1, TS2, and TS3 are the transition states of the surface reaction. TS4 and TS5 are the transition states for surface diffusion. PC1 and PC2 are product complexes. PSS1 and PSS2 are the two product surface sites obtained through the different reaction pathways.

Following the adsorption, H_2O reacts with the Ti intermediate, forming a surface −OH group and releasing an HCl molecule. The energy profile of the surface diffusion and reaction of H_2O on the Ti surface intermediate is shown in Figure 5. Starting from different adsorption states (RC1, RC2, or RC3), the minimum energy reaction pathway leading to the release of HCl is different, while the mechanisms of the different pathways are similar. As the adsorbed H_2O attacks the Ti, the negative

charge of Ti increases with decreasing Ti−O bond distance. Depending on the orientation of the H_2O relative to the Ti group, the rehybridization of Ti (induced by the accumulation of negative charge) leads to the breakage of one of the Ti−Cl bonds, which occurs early along the reaction coordinate. Meanwhile, as the O in H_2O bonds with Ti, the O−H bond closer to the released Cl is weakened with the transfer of negative charge from H to O. The now negatively charged Cl is capable of attacking the positively charged H to break the H−O bond and form HCl. The energies of the transition states TS1, TS2, and TS3 are predicted to be 16.8, 15.8, and 18.9 kcal/mol relative to their corresponding adsorbed complexes, as shown in Figure 5. The two reaction pathways going through the transition state structures TS1 and TS2 give rise to the same product complex, leaving the same surface site (PSS1) after the desorption of HCl. In contrast, the reaction pathway passing through the transition state structure TS3 results in a different surface site (PSS2). This structure (PSS2) is slightly distorted by the attraction between the H atom from the surface −OH group and the O atom from the SiO_2 substrate. The relaxation of the structure from PSS2 to PSS1 is exothermic by 1.7 kcal/mol. As a result of the lower potential energy, the PSS1 surface sites are predicted to be more prevalent than the PSS2 sites. In addition, there are two reaction pathways (with smaller barriers) leading to PSS1 surface sites, while there is only one reaction pathway leading to PSS2 surface sites.

Water molecules can undergo further reactions with the surface intermediates to release additional HCl molecules, until all of the Cl atoms on the surface are replaced by hydroxyl groups. Similar to the atomic mechanism that produced the first hydroxyl group, the subsequent hydroxylation reactions are initiated with the adsorption of H_2O on the surface Ti intermediates. Water molecules can be attached to the top or to the side sites of the Ti intermediates to form an adsorbed complex. Following the adsorption, one H atom from the adsorbed H_2O bonds with the nearest surface Cl atom to form HCl. Although the different adsorption modes of H_2O on Ti can initiate different reaction pathways, atomic mechanisms and associated energies along these reaction pathways are very similar. Therefore, we only consider the reaction pathway starting from the adsorption of H_2O to the apical sites of the Ti groups.

The ZPE-corrected PESs for the three hydroxylation reactions on Ti intermediates are shown in Figure 6. The three hydroxylation reactions leading to the removal of the first, second, and third Cl atoms have almost identical activation barriers (16.8, 16.5, and 16.5 kcal/mol) and are increasingly endothermic (3.5, 5.7, and 7.0 kcal/mol). The overall reaction enthalpy for the removal of all three Cl atoms is 16.2 kcal/mol. Although these reactions are thermodynamically unfavorable, they are still suitable for ALD because of the continuous purge of the gaseous product (HCl). However, the lack of a thermodynamic driving force suggests that the hydroxylation reactions may not be complete (leaving Cl impurities) unless the HCl products are continuously removed from the reactor. Because the product complex is higher in energy than the reactant complex, the reverse exchange reaction features a lower activation barrier than that of the forward hydroxylation reaction. If the adsorbed HCl molecules do not desorb in time or the desorbed HCl molecules readsorb on the surface, the faster reverse reaction can lead to Cl impurities in the film.

3.1.3. Cluster Size Effect. Two different cluster models, shown in Figure 1a,b, were used to represent isolated −OH groups on the surface, to examine the effect of cluster size on the geometry and energy predictions along the reaction coordinate. The

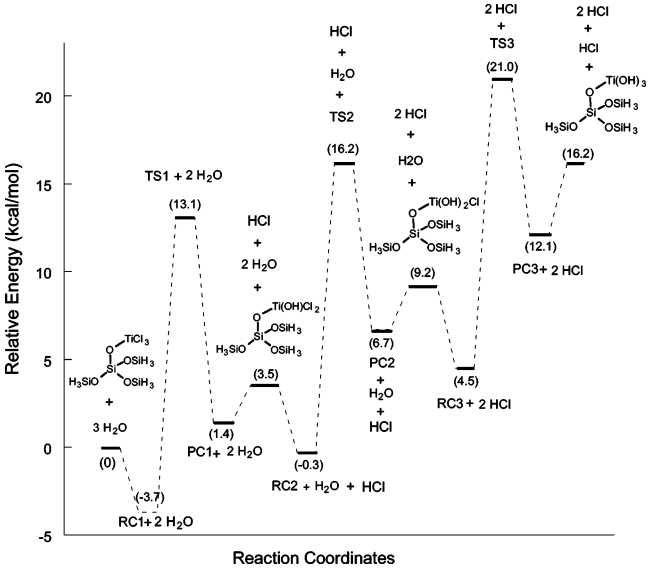

Figure 6. ZPE-corrected PES for the three continuous hydroxylation reactions on the isolated −OH group. RC: reactant complex; TS: transition state; PC: product complex.

TABLE 3: Predicted Relative Energies of the Critical Structures for the SiO_2−OH* + $TiCl_4$ → SiO_2−O−$TiCl_3$* + HCl Half-Reaction Calculated with Two Different Cluster Sizes

	relative energy (kcal/mol)	
	$Si(OH)_3$−OH* cluster	$(SiH_3O)_3Si$−OH* cluster
SiO_2−OH* + $TiCl_4$	0	0
reactant complex	−3.8	−3.2
TS	10.9	8.7
product complex	−7.1	−6.9
SiO_2−O−$TiCl_3$* + HCl	−4.6	−6.5

TABLE 4: Predicted Relative Energies of the Critical Structures for the SiO_2−O−$TiCl_3$* + H_2O → SiO_2−O−Ti(OH)Cl_2* + HCl Half-Reaction Calculated with Two Different Cluster Sizes

	relative energy (kcal/mol)	
	$Si(OH)_3$−OH* cluster	$(SiH_3O)_3Si$−OH* cluster
SiO_2−O−$TiCl_3$* + H_2O	0	0
reactant complex	−3.4	−3.7
TS	13.8	13.1
product complex	−0.3	1.4
SiO_2−O−Ti(OH)Cl_2* + HCl	3.2	3.5

predicted energies of the stationary points on the PESs for the two half-reactions (taking place on an isolated −OH group) are shown in Tables 3 and 4. Although the calculations using the two clusters predict the same reaction mechanism, deviations in energy along the reaction coordinates are observed. For example, the calculated activation barrier of the $Si(OH)_3$−OH* + $TiCl_4$ reaction is 2.8 kcal/mol higher with the small cluster model than with the large cluster model. A closer examination shows that the difference in energy is an artifact from the boundary conditions of the small cluster. Specifically, the interaction between the terminal H atoms and the negatively charged atom in the precursor molecule can distort the geometry and lead to an unrealistic PES. For the $Si(OH)_3$−OH* + $TiCl_4$ reaction, the energy of the adsorbed complex (Figure 7a) is underestimated by using the small cluster due to the interaction between the artificial H-termination and the Cl in $TiCl_4$. In addition, the transition state structure (Figure 7b) is deformed by artificial interactions between H and Cl. The predicted Ti−

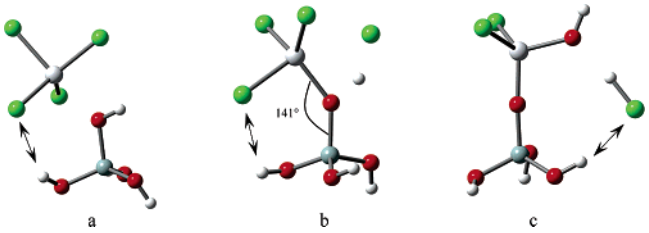

Figure 7. Distorted geometries predicted by using the $Si(OH)_3-OH^*$ cluster.

O−Si bond angle decreases from 146° (large cluster) to 141° (small cluster). This deformation tension leads to an overestimation of the energy of the transition state structure with use of the small cluster.

The deviations in energy due to the boundary effects are also observed for the $SiO_2-O-TiCl_3^* + H_2O$ reaction. As illustrated in Figure 7c, the artificial interaction of H and Cl leads to the underestimation of the energy of the product complex. As a result, the desorption energy of HCl calculated with use of the small cluster is 1.4 kcal/mol higher than that with the large cluster. Therefore, in our calculations, the large $(SiH_3O)_3Si-OH^*$ cluster is used to represent isolated surface −OH groups, to avoid unrealistic boundary effects.

3.2. Adjacent Hydrogen-Bonded Hydroxyl Groups. *3.2.1. First Half-Reaction.* Adjacent hydroxyl groups on the SiO_2 surface can interact through their hydrogen bonds, and reactions taking place on these groups are different from those on isolated hydroxyl groups. $TiCl_4$ can adsorb on the adjacent hydroxyl groups in two modes. The two adsorption states that have been identified are shown in Figure 8a,c. Similar to the reactions on the isolated −OH group, $TiCl_4$ can adsorb on one of the −OH groups through a Lewis acid/base interaction between Ti and O. The adsorption step is weakly exothermic with an adsorption energy of −3.4 kcal/mol, which is very close to that on the isolated −OH group. In addition, $TiCl_4$ can "sit" on the bridge site of the two adjacent −OH groups. A NBO analysis shows that there are strong interactions between the oxygen lone pair NBOs of the two O atoms from the adjacent surface −OH groups and the Ti−Cl antibond NBOs of the adsorbed $TiCl_4$. These interactions lead to donations of occupancy from these oxygen lone pair NBOs into the empty Ti−Cl antibond hybrid orbitals.

A natural population analysis leads to the same conclusion. The total population on all of the NAO of $TiCl_4$ increased by 0.26 in the adsorbed state compared to that in the gas phase. The increase in the NAO population is approximately double that of the $TiCl_4$ adsorbed on an isolated −OH group (0.11). This increase is due to the donation of occupancy from the two oxygen atoms of the adjacent surface −OH groups, which is delocalized in the NAOs of $TiCl_4$. As a result, the adsorption energy of $TiCl_4$ is 6.5 kcal/mol on adjacent −OH surface sites, which is approximately double that on isolated −OH surface sites (3.2 kcal/mol). In addition, the two oxygen lone pairs interact with the adsorbed $TiCl_4$, leading to approximately 6-coordinated Ti and changing the coordination geometry from tetrahedron close to octahedron. DFT calculation results suggest that the bridge-site mode is more stable than the adsorption on a single hydroxyl group. Although the adsorption on the bridge site involves the breakage of the hydrogen bond (which presents an energy barrier), the "hop" barrier for $TiCl_4$ from the single hydroxyl group to the bridge site is very small (1.6 kcal/mol). Therefore, these "hops" are favored thermodynamically, with minimal kinetic limitations, and the bridge-site mode is predicted to be the favored adsorption state.

The reaction mechanism is illustrated in Figure 8. As shown, $TiCl_4$ first adsorbs onto one of the −OH surface sites, and then it easily "hops" to the bridge site to form a more stable adsorption complex. Following the formation of the adsorbed complex, $TiCl_4$ can attack one of the surface −OH groups to release HCl. This process may occur through two potential reaction pathways. As shown in Figure 8c, the H in the hydroxyl group can associate with one of the two closest Cl atoms (Cl1 and Cl2) to form HCl. In each of the two pathways, during the approach of $TiCl_4$, the directions of both the $TiCl_4$ molecule and the −OH groups are adjusted to reduce the distance of H and the targeted Cl. With the decrease of the H−Cl distance, the attraction between H and the targeted Cl increases the distance of Ti and the targeted Cl, weakening the Ti−Cl bond.

Meanwhile, as Ti approaches O, electronic charge is transferred from O to Ti with the formation of the Ti−O bond. The rehybridization of the Ti group, due to its accumulation of negative charge, causes the weakened Ti−Cl bond to break, releasing the negatively charged Cl. During this process, with the electronic charge transfer from O to Ti, the O becomes more electron attractive. This tendency, together with the H−Cl attraction, induces the electronic charge transfer from H to O, weakening the O−H bond. Next, the released negatively charged Cl promptly attacks the positively charged H to form H−Cl, and the system is stabilized through the subsequent relaxation of the structure.

The energy profile for the reaction above is shown in Figure 9. As illustrated in the figure, both reaction pathways lead to the same product with a reaction enthalpy of −3.5 kcal/mol. However, the activation barrier of the reaction via the TS1 transition state structure (14.3 kcal/mol) is much lower than that via the TS2 transition state structure (23.8 kcal/mol). The large difference that we calculate is not surprising. In the adsorption complex, Figure 8c, the H−Cl2 distance is longer than the H−Cl1 distance. Therefore, it requires more energy to distort this structure to reach the transition state, where Cl2 can "see" the H. Even at elevated temperatures, such a difference in activation energies (9.5 kcal/mol) corresponds to a large difference in reaction rates. Hence, the reaction via the TS1 transition state structure with the lower activation barrier is considered to be the dominant reaction path.

After liberating one HCl, the remaining Ti intermediate on the surface can further react with the adjacent surface hydroxyl groups. The reaction mechanism (Figure 8) is similar to the first exchange reaction. The H in the hydroxyl group can bond to the nearest Cl to liberate an HCl molecule, leaving a Ti intermediate bonded to the two surface O atoms. As illustrated in the energy profile (Figure 9), the activation barrier of the reaction with the second hydroxyl group is 14.8 kcal/mol, which is very close to that of the exchange reaction with the first hydroxyl (14.3 kcal/mol). However, the first exchange reaction has a reaction enthalpy of −3.5 kcal/mol, while the reaction with the second hydroxyl group is endothermic by 3.9 kcal/mol. The overall reaction enthalpy of the reaction between the $TiCl_4$ and the two adjacent hydroxyl groups is 0.4 kcal/mol.

As a result of the nonequilibrium nature of ALD, kinetics plays a key role in determining the structure and homogeneity of the deposited film. According to the results of our DFT calculations, the first-half reactions on isolated and adjacent hydroxyl groups feature similar reaction barriers indicating similar intrinsic kinetics.

3.2.2. Second Half-Reaction. When the second precursor (H_2O) is introduced onto the surface, the surface intermediates deposited during the first half-cycle (Figure 8k) can be fully

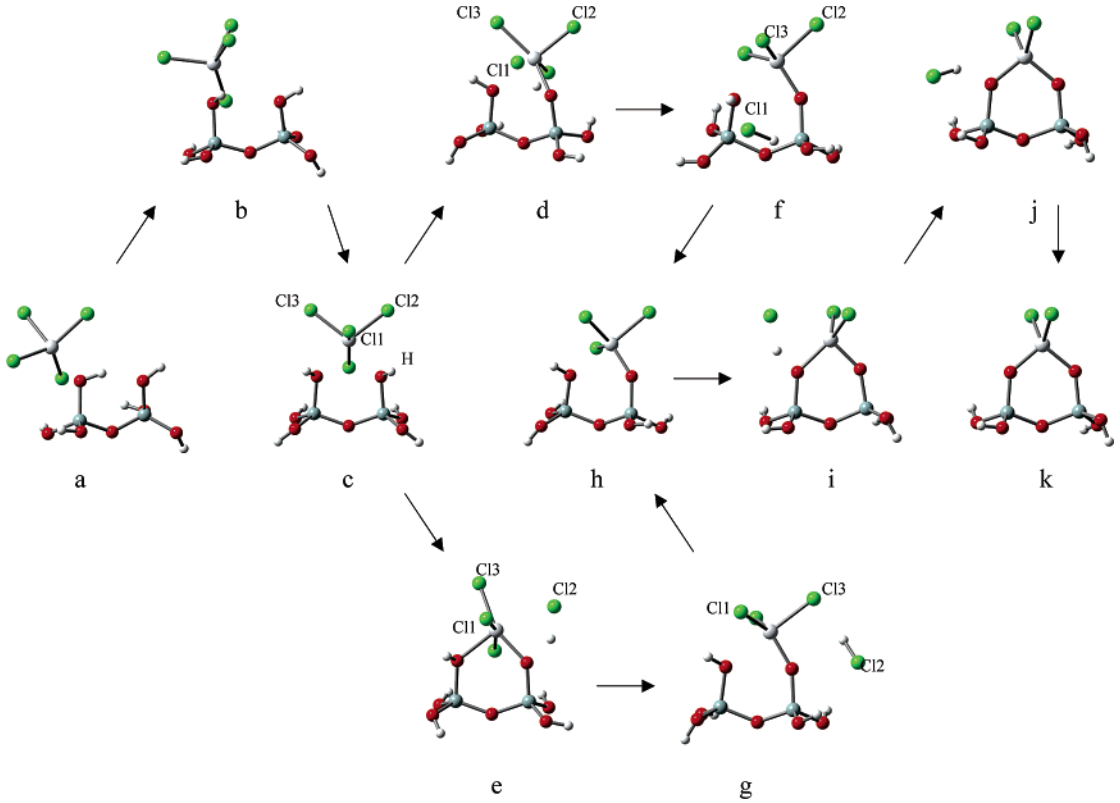

Figure 8. Atomic mechanism of the reaction between $TiCl_4$ and adjacent hydrogen-bonded hydroxyl groups on the SiO_2 surface: (a) adsorption on a single hydroxyl group, (b) transition state structure for $TiCl_4$ diffusion between the two adsorption states, (c) adsorption on the bridge site, (d) transition state structure, (e) transition state structure, (f) product complex, (g) product complex, (h) surface intermediate after the desorption of HCl, (i) transition state structure, (j) product complex, and (k) surface intermediate after the desorption of HCl.

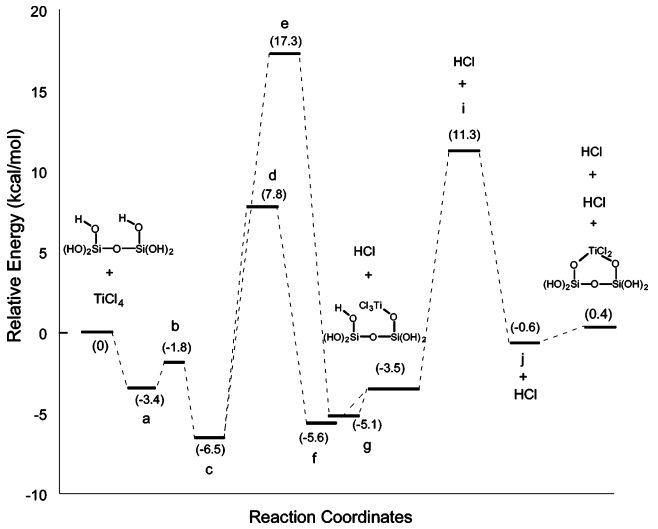

Figure 9. ZPE-corrected PES for the first half-reactions taking place on the adjacent hydrogen-bonded −OH groups. The letters correspond to the structures shown in Figure 8.

hydroxylated with the removal of the surface Cl atoms. The reaction mechanism, with the associated energetics, is shown in Figure 10. Similar to the $H_2O + SiO_2{-}O{-}TiCl_3$* reaction described above, H_2O molecules first adsorb onto the surface Ti intermediate. Following the formation of the adsorbed complex, the adsorbed H_2O is capable of attacking the Ti group to release an HCl molecule, leaving a surface hydroxyl group bonded to Ti. The atomic mechanism is similar to that of the $H_2O + SiO_2{-}O{-}TiCl_3$* reaction described above. After the first hydroxylation reaction, the remaining surface Cl can react with another H_2O molecule to form a second surface hydroxyl

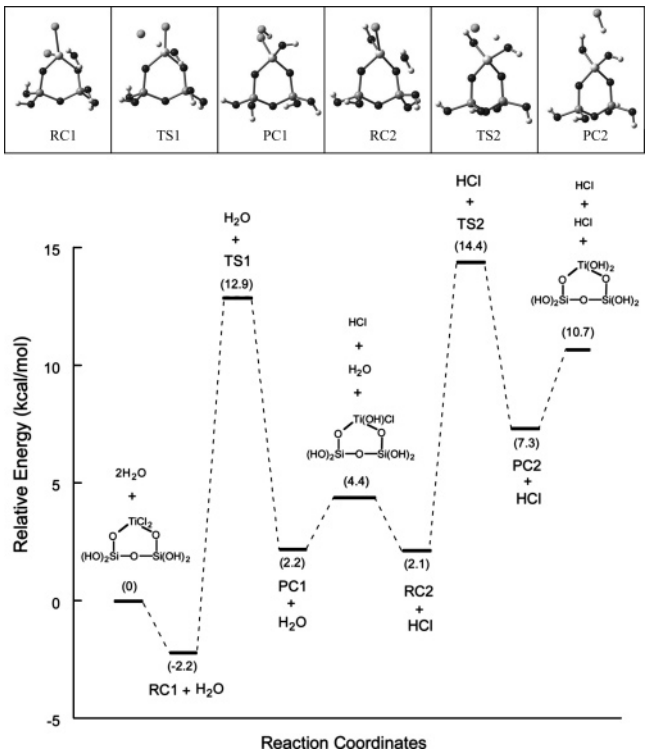

Figure 10. ZPE-corrected PES for the two continuous hydroxylation reactions during the second half-reactions on the adjacent −OH groups.

group. Comparison of these two hydroxylation reactions indicates very similar H_2O adsorption energies (2.2 and 2.3 kcal/mol). However, the activation barrier to remove the second Cl atom (12.3 kcal/mol) is lower than that of the first hydroxylation reaction (15.1 kcal/mol). Similar to the $H_2O + SiO_2{-}O{-}TiCl_3$*

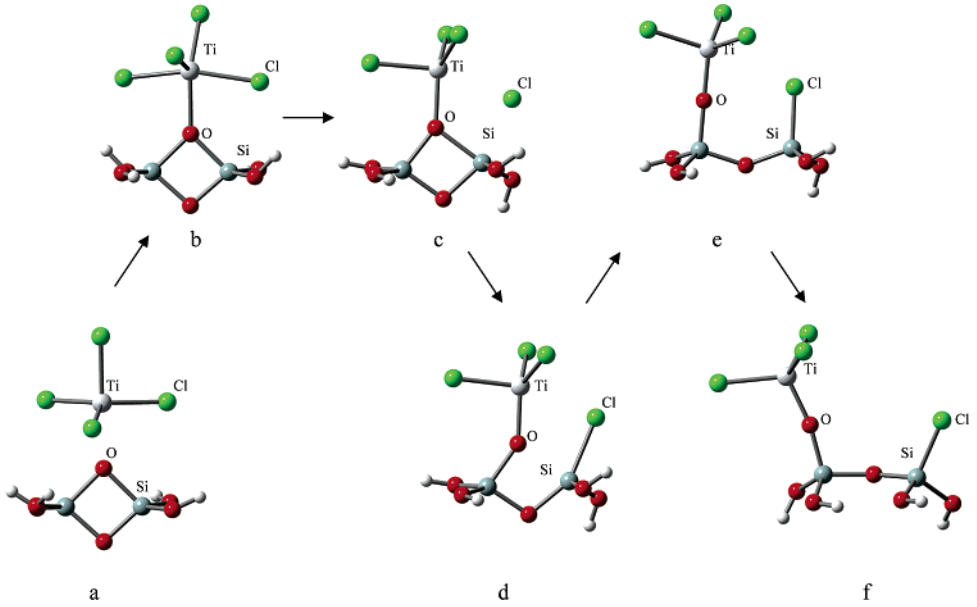

Figure 11. Atomic mechanism of the reaction between $TiCl_4$ and oxygen bridge sites: (a) reactant complex, (b) formation of the Ti−O bond and a 5-coordinated Ti, (c) breaking of the Ti−Cl bond, (d) transition state structure, (e) relaxation of the structure, and (f) product complex.

reaction, these two hydroxylation reactions are endothermic. The overall reaction enthalpy of the two continuous hydroxylation reactions is 10.7 kcal/mol. Considering the endothermic nature of this step, the second half-reaction favors the removal of the HCl product and enough exposure time will drive the hydroxylation reactions to completion, reducing Cl impurities.

3.3. Oxygen Bridges. In addition to reactions with the surface hydroxyl groups, the $TiCl_4$ precursor molecules can also react with oxygen bridges on the surface. The reaction mechanism is illustrated in Figure 11. Similar to the first half-reactions on the surface hydroxyl groups, $TiCl_4$ first spontaneously adsorbs on the surface oxygen bridges through a Lewis acid/base interaction between Ti and O. This step is weakly exothermic with an adsorption energy of −4.7 kcal/mol. The adsorbed $TiCl_4$ is then capable of attacking the reactive oxygen bridges. As Ti approaches O, negative charge is transferred from O to Ti with the creation of a Ti−O bond. The accumulation of negative charge on Ti can induce the rehybridization of the Ti group from 5-coordination to 4-coordination, which causes a Ti−Cl bond to break, releasing a negatively charged Cl. Meanwhile, with the electronic charge transfer from O to Ti, the O becomes more electron attractive. This tendency, together with the Si−Cl attraction, induces the electronic charge transfer from Si to O, weakening Si−O bond (closest to the negatively charged Cl). The negatively charged Cl is then capable of attacking the positively charged Si to break the Si−O bond and form a Si−Cl bond. When the system passes through the transition state structure along the reaction coordinate, the structure promptly relaxes by swinging out the Ti group and relaxing the Si−O−Si angle. The energy profile for the reaction above is shown in Figure 12. As noted in the figure, the reaction is exothermic by 27.9 kcal/mol with the activation barrier of 12.8 kcal/mol. As compared to the exchange reaction of $TiCl_4$ on surface hydroxyl groups, the reaction between $TiCl_4$ and surface oxygen bridges has a similar activation barrier (12.8 kcal/mol on oxygen bridges versus 11.9 kcal/mol on isolated hydroxyl groups and 14.3 kcal/mol on adjacent hydrogen-bonded hydroxyl groups), but the reaction is much more exothermic.

On the basis of the nearly equivalent activation barriers, we predict that the reactivity of the oxygen bridges will be very similar to that of the hydroxyl groups. However, this conclusion

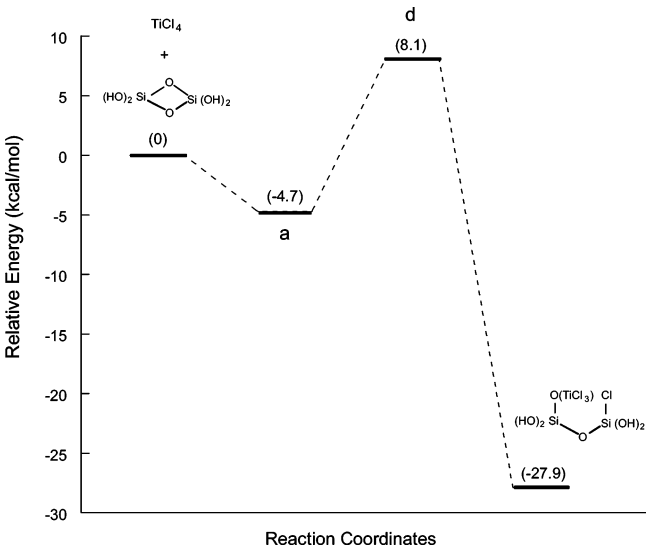

Figure 12. ZPE-corrected PES for the reaction between $TiCl_4$ and the oxygen bridges sites. The labels "a" and "d" correspond to the structures shown in Figure 11.

is contrary to the measurements of Kinney and Staley,[30] who observe that the siloxane bridges react with $TiCl_4$ more quickly than the hydroxyl groups. We believe that this discrepancy is the result of the experimental conditions used. In the experiments, $TiCl_4$ was filled into a sealed chamber containing the silica sample, and their conclusion was drawn from the FTIR spectrum collected after the reactions reached *equilibrium*. As the reaction enthalpy (ΔH_0) for the reaction of $TiCl_4$ on the surface oxygen bridges (−27.9 kcal/mol) is much more negative than the ΔH_0 for the exchange reaction on the hydroxyl groups (−6.5 kcal/mol on isolated hydroxyl groups and −3.5 kcal/mol on adjacent hydrogen-bonded hydroxyl groups), the equilibrium constant of the reaction on the oxygen bridges is predicted to be significantly larger than that on the hydroxyl groups. This large difference in equilibrium constants indicates that the extent of reaction on the oxygen bridges is higher than that on the surface hydroxyl groups. Therefore, it is not surprising to observe a larger fraction of oxygen bridges reacted with $TiCl_4$ than surface hydroxyl groups *at equilibrium*. However, the

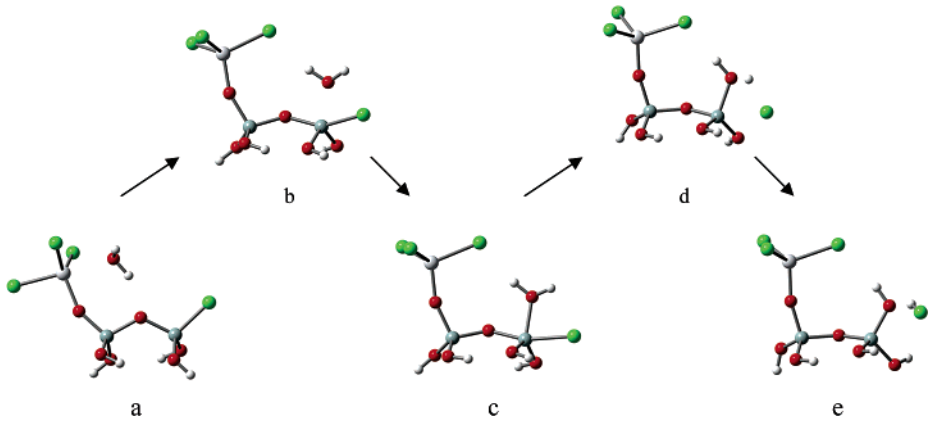

Figure 13. Atomic mechanism of the $H_2O + SiO_2-Cl^*$ reaction: (a) adsorbed reactant complex, (b) first transition state structure, (c) reaction intermediate, (d) second transition state structure, and (e) adsorbed product complex.

equilibrium thermodynamics does not yield information pertinent to the individual reaction rates. Considering the nonequilibrium nature of ALD, where reverse reactions are often negligible, we believe that an in situ analysis will show a simultaneous and proportional decrease in the number of oxygen bridges and hydroxyl groups during exposure to $TiCl_4$.

3.4. Surface Chlorine. The reaction between $TiCl_4$ and surface oxygen bridges leaves two adjacent, dissimilar surface groups: $SiO_2-O-TiCl_3^*$ and SiO_2-Cl^* (Figure 11f). The $SiO_2-O-TiCl_3^*$ group is similar to the surface intermediate formed by the reaction between $TiCl_4$ and the isolated surface hydroxyl group, and the reaction between H_2O and this type of surface group has been described above. So, although both of the surface groups can react during the H_2O exposure, here we only examine the reaction between H_2O and SiO_2-Cl^*.

When introduced into the reactor, H_2O first spontaneously absorbs onto the $SiO_2-O-TiCl_3^*$ surface site through a Lewis acid/base interaction between Ti and O. Similar to our previous calculations, there are three different adsorption modes (RC1, RC2, and RC3). Although the exchange reaction between H_2O and $SiO_2-O-TiCl_3^*$ can begin from any of these three adsorption states, we only found a single $H_2O + SiO_2-Cl^*$ reaction pathway, initiated from the RC3 adsorption state. However, possible reaction pathways starting from the other adsorption states may be found by using larger cluster modes, which takes into account different combinations of neighboring groups. This possibility will be investigated in future studies.

The atomic mechanism of the $H_2O + SiO_2-Cl^*$ reaction is shown in Figure 13. As illustrated in the figure, H_2O first spontaneously absorbs onto the $SiO_2-O-TiCl_3^*$ surface site through the RC3 adsorption mode. Following the formation of the adsorption complex, the adsorbed H_2O is capable of attacking the Ti group to release a HCl and leave a surface hydroxyl group bonded to Ti. As an alternative to the $H_2O + SiO_2-O-TiCl_3^*$ pathway, the adsorbed H_2O may attack the adjacent SiO_2-Cl^* group. The lone pair on the aqueous oxygen is capable of attacking the surface Si in a nucleophilic fashion. As the H_2O approaches the SiO_2-Cl^* group, it adjusts its direction so that the aqueous oxygen can directly attack the silicon and form a Si−O bond through the TS1 transition state, a process that is accompanied by the extrusion of the surface Cl. As noted in the energy profile (Figure 14), the activation barrier of this step is 17.8 kcal/mol.

Due to the poor electrophilicity of the SiO_2-Cl^* group, the reaction intermediate (Figure 13c) is 17.1 kcal/mol higher in energy than adsorbed reactant complex (Figure 13a). With the formation of the Si−O bond, the rehybridization of Si (induced

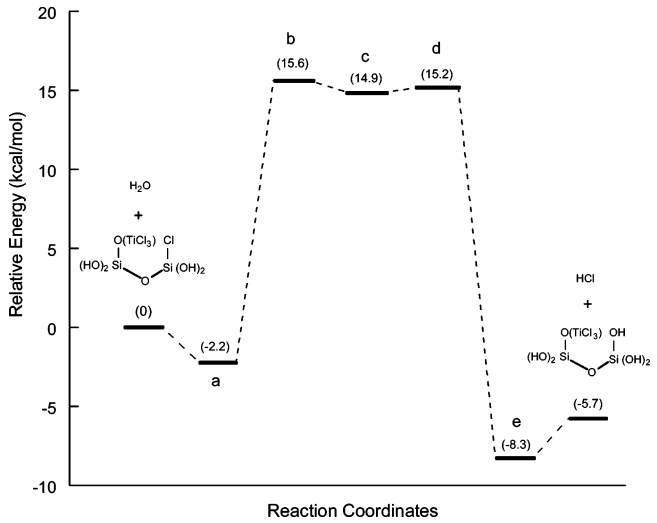

Figure 14. ZPE-corrected PES for the $H_2O + SiO_2-Cl^*$ reaction. The letters correspond to the structures shown in Figure 13.

by the negative charge transfer from O to Si) leads to the breakage of the Si−Cl bond. Meanwhile, the rehybridization of Si stabilizes the transfer of negative charge in the H_2O molecule from one H to O. The now negatively charged Cl is capable of attacking the positively charged H to break the H−O bond and form HCl, and this step occurs easily with a very small barrier (0.3 kcal/mol). Different from the endothermic $H_2O + SiO_2-O-TiCl_3^*$ reaction, the overall $H_2O + SiO_2-Cl^*$ reaction is exothermic by 5.7 kcal/mol.

As mentioned above, after the adsorption on the $SiO_2-O-TiCl_3^*$ surface site, H_2O can react with either $SiO_2-O-TiCl_3^*$ or the adjacent SiO_2-Cl^* group. In the competing reactions the reactant is consumed by two different reactions to form different products:

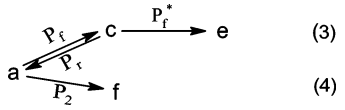

where **a**, **c**, and **e** represent the structures denoted by the same letters in Figure 13, **f** represents the adsorbed product complex of the $H_2O + SiO_2-O-TiCl_3^*$ reaction, and P_f, P_r, P_f^*, and P_2 denote the probabilities of the corresponding reactions. As the HCl product is assumed to be removed, the reverse reactions (from **e** to **c** and from **f** to **a**) are neglected. In the consecutive $H_2O + SiO_2-Cl^*$ reaction (reaction 3), the reactant forms an intermediate product **c**, which either reacts further to form the

final product **e** or back to reactant **a**. The probability of the specific reaction event i (P_i) is proportional to $\exp(-\Delta G_i/RT)$, where ΔG_i is the free energy of activation of reaction i. Assuming that the difference in entropy between the transition state and the reactant complex (ΔS_i) is negligible and that ΔH_i only changes slightly as a function of temperature (at moderate temperatures), P_i is approximately proportional to $\exp(-\Delta H_{i0}/RT)$, where ΔH_{i0} is the enthalpy of activation at 0 K. As illustrated in Figure 14, ΔH_{i0} of the reactions from **c** to **e** and from **c** to **a** is 0.3 and 0.7 kcal/mol, respectively. At a temperature of 500 K, we can estimate the branching ratio of these two reactions:

$$\frac{P_f^*}{P_r} = 1.5 \tag{5}$$

reaction 3 proceeds through the formation of a relatively unstable, short-lived intermediate **c**, whose transformation rate is orders of magnitude faster than the rates of other reactions taking place on the reactive site. Therefore, we can assume that the short-lived intermediate **c** is in the steady state. From this assumption, we obtain:

$$P_f = P_r + P_f^* \tag{6}$$

The overall probability of reaction 3 resulting from this assumption is then obtained by combing eqs 5 and 6:

$$P_1 = P_f - P_r = 0.6P_f \tag{7}$$

According to the calculations for the reaction of H_2O on the isolated $SiO_2-O-TiCl_3$* group, the activation barrier of reaction 4 starting from the RC3 adsorption state is 18.9 kcal/mol. Additionally, as shown in Figure 14, the activation barrier of the reaction from **a** to **c** is 17.8 kcal/mol. Therefore, we can estimate the relative probability of reactions 3 and 4:

$$\frac{P_1}{P_2} = 0.6\frac{P_f}{P_2} = 1.8 \tag{8}$$

This result indicates that, after the adsorption on the $SiO_2-O-TiCl_3$* surface site in the RC3 adsorption mode, H_2O reacts with the adjacent SiO_2-Cl* group more likely than with the $SiO_2-O-TiCl_3$* group. However, it cannot be concluded that the H_2O prefers the SiO_2-Cl* group, since there are two alternate pathways involving $H_2O + SiO_2-O-TiCl_3$*, with relatively small barriers (starting from the RC1 and RC2 adsorption states of H_2O).

4. Conclusions

The initial reaction mechanisms for TiO_2 ALD onto SiO_2 surfaces, using $TiCl_4$ and H_2O as precursors, have been investigated with DFT calculations. The detailed atomic growth mechanisms on different types of reactive groups of the SiO_2 surface (isolated −OH groups, adjacent hydrogen-bonded −OH groups, and surface oxygen bridges) are different. During each exposure, the gaseous precursor ($TiCl_4$ or H_2O) can react with different types of reactive groups through different reaction pathways, leaving various products on the surface.

When dosed into the reactor, the $TiCl_4$ can react with isolated hydroxyl groups to leave a $SiO_2-O-TiCl_3$* species, with an activation barrier of 11.9 kcal/mol. Meanwhile, $TiCl_4$ can also react with adjacent hydrogen-bonded hydroxyl groups to leave a $TiCl_2$* surface group. The dominant reaction mechanisms for these steps have been identified, and the activation barriers of the two consecutive reactions (releasing two HCl molecules) are 14.3 and 14.8 kcal/mol. In addition, with a barrier of 12.8 kcal/mol, $TiCl_4$ can react with surface oxygen bridge to leave two adjacent surface groups ($SiO_2-O-TiCl_3$* and SiO_2-Cl*). Our calculations indicate that all of the investigated surface functionalities are reactive toward the $TiCl_4$ precursors.

During the second-half cycle, which introduces H_2O into the reactor, all of these intermediate surface groups can then react with H_2O. Multiple adsorption modes of H_2O on the $SiO_2-O-TiCl_3$* surface group have been found, and the predicted adsorption energies of the different adsorption modes are all very similar. The "hop" barriers of adsorbed H_2O among the different adsorption states are very small, indicating rapid equilibration among these modes, and these adsorption modes can initiate different reaction pathways. The $SiO_2-O-TiCl_3$* surface group can react with three consecutive H_2O molecules to release three HCl molecules, leaving $SiO_2-O-Ti(OH)_3$* on the surface. The activation barriers of these three consecutive hydroxylation reactions are similar (16.8, 16.5, and 16.5 kcal/mol). Similarly, H_2O can continuously react with the surface $TiCl_2$* group to release two HCl molecules and form a surface $Ti(OH)_2$* group. The activation barriers of these two consecutive exchange reactions are 15.1 and 12.3 kcal/mol. In addition, an atomic mechanism of the H_2O and SiO_2-Cl* reaction has been investigated. This reaction starts with the adsorption of H_2O on the adjacent $SiO_2-O-TiCl_3$* surface site in the RC3 adsorption mode. After the adsorption, the adsorbed H_2O is predicted to prefer the reaction with the adjacent SiO_2-Cl* group over that with the $SiO_2-O-TiCl_3$* group. The $H_2O + SiO_2-Cl$* reaction is a consecutive reaction with the formation of an unstable product intermediate, and the primary activation barrier of this reaction is 17.8 kcal/mol.

Our DFT calculations show the complexity of the growth mechanisms during TiO_2 ALD. The concentration and arrangement of the different surface reactive groups determine the resulting film growth characteristics. Therefore, the factors which are related to the presence of the different surface reactive groups, such as configuration of initial SiO_2 substrate and growth temperature, are predicted to have a marked influence on film structure and growth rate. If reproducibility is expected, experimental investigations should begin with thoroughly characterized substrates, and the resulting film deposition must be interpreted with respect to both the equilibrium and the kinetic characteristics of the surface reactions. It is important that our DFT results be interpreted within the context of our cluster models. Other factors, not accounted for here, may influence the predicted reaction mechanisms, such as varying surface coverage and adsorbate−adsorbate interactions. In future work, we plan to incorporate our DFT results into larger simulation models, such as with kinetic Monte Carlo.

Acknowledgment. The authors thank Prof. Tonya Klein for helpful discussions of the experimental systems. This work was partially supported with the computing resources at the Alabama Supercomputer Center.

References and Notes

(1) Halls, M. D.; Raghavachari, K. *J. Chem. Phys.* **2003**, *118*, 10221.

(2) Akamatsu, K.; Kimura, A.; Matsubara, H.; Ikeda, S.; Nawafune, H. *Langmuir* **2005**, *21*, 8099.

(3) King, J. S.; Heineman, D.; Graugnard, E.; Summers, C. J. *Appl. Surf. Sci.* **2005**, *244*, 511.

(4) King, J. S.; Graugnard, E.; Summers, C. J. *Adv. Mater.* **2005**, *17*, 1010.

(5) Kim, Y. S.; Yun, S. J. *J. Cryst. Growth* **2005**, *274*, 585.

(6) Mayer, T. M.; Elam, J. W.; George, S. M.; Kotula, P. G.; Goeke, R. S. *Appl. Phys. Lett.* **2003**, *82*, 2883.
(7) Nistorica, C.; Liu, J. F.; Gory, I.; Skidmore, G. D.; Mantiziba, F. M.; Gnade, B. E.; Kim, J. *J. Vac. Sci. Technol. A* **2005**, *23*, 836.
(8) Elam, J. W.; Routkevitch, D.; Mardilovich, P. P.; George, S. M. *Chem. Mater.* **2003**, *15*, 3507.
(9) Xiong, G.; Elam, J. W.; Feng, H.; Han, C. Y.; Wang, H. H.; Iton, L. E.; Curtiss, L. A.; Pellin, M. J.; Kung, M.; Kung, H.; Stair, P. C. *J. Phys. Chem. B* **2005**, *109*, 14059.
(10) Pellin, M. J.; Stair, P. C.; Xiong, G.; Elam, J. W.; Birrell, J.; Curtiss, L.; George, S. M.; Han, C. Y.; Iton, L.; Kung, H.; Kung, M.; Wang, H. H. *Catal. Lett.* **2005**, *102*, 127.
(11) Liu, S.; Chen, A. *Langmuir* **2005**, *21*, 8409.
(12) Estéve, A.; Jeloaica, L.; Mazaleyrat, G.; Dkhissi, A.; Djafari-Rouhani, M.; Messaoud, A.; Fazouan, N. *MRS Fall Symp. Proc.* **2003**, *786*, E6.28.
(13) Mazaleyrat, G.; Estéve, A.; Jeloaica, L.; Djafari-Rouhani, M. *Comput. Mater. Sci.* **2005**, *33*, 74.
(14) Han, J. H.; Gao, G. L.; Widjaja, Y.; Garfunkel, E.; Musgrave, C. B. *Surf. Sci.* **2004**, *550*, 199.
(15) Frisch, M. J.; Trucks, G. W.; Schlegel, H. B.; Scuseria, G. E.; Robb, M. A.; Cheeseman, J. R.; Montgomery, J. A., Jr.; Vreven, T.; Kudin, K. N.; Burant, J. C.; Millam, J. M.; Iyengar, S. S.; Tomasi, J.; Barone, V.; Mennucci, B.; Cossi, M.; Scalmani, G.; Rega, N.; Petersson, G. A.; Nakatsuji, H.; Hada, M.; Ehara, M.; Toyota, K.; Fukuda, R.; Hasegawa, J.; Ishida, M.; Nakajima, T.; Honda, Y.; Kitao, O.; Nakai, H.; Klene, M.; Li, X.; Knox, J. E.; Hratchian, H. P.; Cross, J. B.; Bakken, V.; Adamo, C.; Jaramillo, J.; Gomperts, R.; Stratmann, R. E.; Yazyev, O.; Austin, A. J.; Cammi, R.; Pomelli, C.; Ochterski, J. W.; Ayala, P. Y.; Morokuma, K.; Voth, G. A.; Salvador, P.; Dannenberg, J. J.; Zakrzewski, V. G.; Dapprich, S.; Daniels, A. D.; Strain, M. C.; Farkas, O.; Malick, D. K.; Rabuck, A. D.; Raghavachari, K.; Foresman, J. B.; Ortiz, J. V.; Cui, Q.; Baboul, A. G.; Clifford, S.; Cioslowski, J.; Stefanov, B. B.; Liu, G.; Liashenko, A.; Piskorz, P.; Komaromi, I.; Martin, R. L.; Fox, D. J.; Keith, T.; Al-Laham, M. A.; Peng, C. Y.; Nanayakkara, A.; Challacombe, M.; Gill, P. M. W.; Johnson, B.; Chen, W.; Wong, M. W.; Gonzalez, C.; Pople, J. A. *Gaussian 03*, revision C.02; Gaussian, Inc.: Wallingford, CT, 2004.
(16) Becke, A. D. *J. Chem. Phys.* **1993**, *98*, 5648.
(17) Lee, C. T.; Yang, W. T.; Parr, R. G. *Phys. Rev. B* **1988**, *37*, 785.
(18) Heyman, A.; Musgrave, C. B. *J. Phys. Chem. B* **2004**, *108*, 5718.
(19) Widjaja, Y.; Han, J. H.; Musgrave, C. B. *J. Phys. Chem. B* **2003**, *107*, 9319.
(20) Widjaja, Y.; Musgrave, C. B. *Appl. Phys. Lett.* **2002**, *81*, 304.
(21) Jeloaica, L.; Estéve, A.; Rouhani, M. D.; Estéve, D. *Appl. Phys. Lett.* **2003**, *83*, 542.
(22) Xu, Y.; Musgrave, C. B. *Chem. Mater.* **2004**, *16*, 646.
(23) Halls, M. D.; Raghavachari, K. *J. Phys. Chem. A* **2004**, *108*, 2982.
(24) Eriksson, L. A.; Pettersson, L. G. M.; Siegbahn, P. E. M.; Wahlgren, U. *J. Chem. Phys.* **1995**, *102*, 872.
(25) Santiso, E.; Gubbins, K. E. *Mol. Simul.* **2004**, *30*, 699.
(26) Hariharan, P. C.; Pople, J. A. *Theor. Chim. Acta* **1973**, *28*, 213.
(27) Blaudeau, J. P.; McGrath, M. P.; Curtiss, L. A.; Radom, L. *J. Chem. Phys.* **1997**, *107*, 5016.
(28) Krishnan, R.; Binkley, J. S.; Seeger, R.; Pople, J. A. *J. Chem. Phys.* **1980**, *72*, 650.
(29) Boys, S. F.; Bernardi, F. *Mol. Phys.* **1970**, *19*, 553.
(30) Kinney, J. B.; Staley, R. H. *J. Phys. Chem.* **1983**, 3735.